INSTITUTE OF PHYSICS PUBLISHING JOURNAL OF PHYSICS D: APPLIED PHYSICS
J. Phys. D: Appl. Phys. **36** (2003) 288–293 PII: S0022-3727(03)54110-9

Stress induced conditioning and thermal relaxation in the simulation of quasi-static compression experiments

M Scalerandi[1], P P Delsanto[1] and P A Johnson[2]

[1] INFM, Dip. Fisica, Politecnico di Torino, Torino, Italy
[2] Los Alamos Nat. Lab, Non Linear Elasticity, Los Alamos, NM, 87545, USA

Received 30 September 2002
Published 15 January 2003
Online at stacks.iop.org/JPhysD/36/288

Abstract
Local interaction simulation approach simulations of the ultrasonic wave propagation in multi-grained materials have succeeded in reproducing most of the recently observed nonclassical nonlinear effects, such as stress–strain hysteresis and discrete memory in quasi-static experiments and a downwards shift of the resonance frequency and the generation of odd harmonics at specific amplitude rates in dynamics experiments. By including a simple mechanism of thermally activated random transitions, we can predict the occurrence of experimentally observed effects, such as the conditioning and relaxation of the specimen. Experiments are also suggested for a quantitative assessment of the validity of the model.

1. Introduction

Recent experimental studies [1–3] have clearly shown that a variety of materials, such as rocks, concrete, elastic materials with mesoscopic defects, etc share a same peculiar elastic behaviour, despite very different microstructure and chemistry. In such materials nonclassical nonlinear effects manifest themselves in both quasi-static [4] and dynamic experiments [2, 5]. A most striking feature is the so-called 'slow dynamics', which consists in a downshift of the resonance frequency when the specimen has been dynamically excited, and consequent recovery proportional to the logarithm of elapsed time [6].

A similar effect is found in quasi-static experiments, where typical hysteretic loops are observed. However, before obtaining them in a stable (repeatable) way, several conditioning stress cycles with increasing residual deformations must be performed. And, if the applied stress is kept constant during or at the end of the experiment, the strain slowly decays and eventually the stress–strain curve falls down over one of the conditioning cycles.

All these effects may be related to the presence of mesoscopic features, which may be considered as bonding regions with specific nonlinear elastic properties. Typical examples are defects and/or interstices among grains in a polycrystalline aggregate or in a granular material. For example, it is well known that, when microscopic contacts are present, dislocations and static friction effects may modify the material strength [6, 7]. Therefore, the application of an external forcing (conditioning) may result in the accumulation of deformation energy in the proximity of contact areas, such as in the case of delaminations or contacts between grain tips. If the energy becomes sufficiently large, rupture of some bonds may occur, with consequent effects at a macroscopic level [8]. The 'activation energy' is generally different for the different kinds of bonds and asymmetric, i.e. different energies are required for restoring vs breaking the bonds. Furthermore, thermal relaxations may induce additional modifications in the bonds structure.

While the traditional nonlinear (Landau) [9] theory is not sufficient to describe these nonlinear phenomena [10, 11], they may be well reproduced by models [12, 13] based on the local interaction simulation approach (LISA) [14, 15], applied in conjunction with a Spring Model approach and a Preisach-Mayergoitz (PM) representation [11, 16]. In this approach, the specimen is described as a sequence of elastic elements, the 'grains', and nonclassical regions corresponding to the interstices, also called hysteretic mesoscopic units (HMUs). The latter behave either rigidly or elastically, depending on the local pressure. To describe this behaviour we have introduced a two-values state variable r which defines the state of the HMU. The resulting model has allowed us to obtain most of the effects observed experimentally both in the dynamic [12] and quasi-static [13] case.

The purpose of the present contribution is to show that thermal fluctuations between the two above mentioned states may be used to predict conditioning and slow dynamics effects, in agreement with experimental observations. In the next section, we briefly describe the model which, although based on phenomenological considerations rather than on the physical properties and specific parameters of a real material, is, in our opinion, general and flexible enough, to provide a suitable tool for the introduction of realistic interaction forces. In the following section, we present a few results of virtual quasi-static experiments, to be compared with the results of real experiments in order to demonstrate the reliability of the model. An application to dynamic experiments is forthcoming.

2. The model

Let us consider a bar of a multi-grained material and assume that all the grains have equal length ε, are homogeneous and somewhat aligned. The specimen may then be represented by a one-dimensional lattice, as sketched in figure 1(a), i.e. as a sequence of elastic portions (the grains), each of mass m, separated by massless interstice regions (the HMU's defined in the introduction). Following the Spring Model approach [15], each grid node i is split into two sub-nodes $i^{\pm}$, which delimit the corresponding HMU.

We then assume that an ultrasonic pulse (or wave) travels along the specimen acting upon each node i by means of two elastic 'external forces' $F_i^+(t)$ and $F_i^-(t)$, applied to the two sub-nodes i^+ and i^- from the right- and left-hand side, respectively (see figure 1(a)). As a consequence the two sub-nodes undergo the displacements $u_i^+(t)$ and $u_i^-(t)$. Associating to each sub-node a mass $m/2$, it follows

$$\tfrac{1}{2}m\ddot{u}_i^{\pm} = F_i^{\pm} - \gamma\dot{u}_i^{\pm} \mp f_i \tag{1}$$

where γ is the attenuation coefficient in each grain and f_i is an internal force (to be specified later) whose task is to keep the two sub-nodes together. Next we define the HMU centre-of-mass displacement $u_i(t) = (u_i^+ + u_i^-)/2$ and length $\delta_i(t) = u_i^+ - u_i^-$. For the former equations (1) yield immediately

$$m\ddot{u}_i = F_i^+ + F_i^- - 2\gamma\dot{u}_i \tag{2}$$

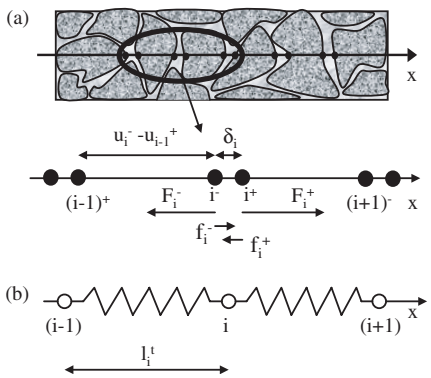

Figure 1. (a) One-dimentional lattice representation of the bar. The black dots represent the sub-nodes delimiting the HMU's. (b) Simplified lattice with varying spring rest-lengths $l_i(t)$.

Assuming that each grain has a constant 'equilibrium' length ε_0 and stiffness S, we can write the external forces as

$$F_i^{\pm}(t) = S(u_{i\pm1}^{\mp} - u_i^{\pm}) \tag{3}$$

It is interesting to observe that, since

$$u_i - u_{i-1} - \tfrac{1}{2}(\delta_i + \delta_{i-1}) = u_i^- - u_{i-1}^+ \tag{4}$$

we have

$$F_i^{\pm}(t) = S\left(u_{i\pm1} - u_i - \tfrac{1}{2}(\delta_i + \delta_{i-1})\right) \tag{5}$$

Therfore, it is possible to interpret equation (5) as the elastic force due to a spring with

$$l_i(t) = \varepsilon_0 + \tfrac{1}{2}(\delta_i + \delta_{i-1}) \tag{6}$$

as a varying rest-length in a simplified lattice (see figure 1(b)).

In order to find an equation for $\delta_i(t)$, we must include in the model the 'internal' bonding forces f_i, which, as mentioned in the introduction, are assumed to leave the HMU in one of two possible states, according to the value of the state variable r_i.

- Rigid bond case, defined by the value $r_i = 0$ of the state variable. In this case, $\ddot{\delta}_i = \dot{\delta}_i = 0$, δ_i does not change and the pulse propagates unaffected by the HMU.
- Variable HMU length case, defined by $r_i = 1$. In this case, the two sub-nodes may drift apart or get indefinitely closer, and a restoring elastic force (with coefficient K_i) is needed to take into account the 'resistance' opposed, e.g. by the surrounding grains of the specimen to a variation of δ_i from its 'equilibrium' value $\delta_i(0)$.

The two cases considered can be both represented by the equation (which implicitely includes the internal forces)

$$\tfrac{1}{2}m\ddot{\delta}_i = r_i(Q_iP_i - \gamma\dot{\delta}_i - K_i(\delta_i - \delta_i(0))) \qquad r_i = 0, 1 \tag{7}$$

where

$$P_i = F_i^+ - F_i^- \tag{8}$$

is the pressure applied to the interstice and Q_i is a model parameter ($0 \leqslant Q_i \leqslant 1$) used to describe the quality of the bond region. According to equation (7), the internal forces are defined in the present model as:

$$f_i = \tfrac{1}{2}\left[(Q_i - 1)\,P - K_i\,(\delta_i - \delta_i(0))\right] \qquad \text{non rigid case}$$
$$f_i = -\tfrac{1}{2}P \qquad \text{rigid bond case} \tag{9}$$

Omitting for brevity the index i, the state variable r for each individual HMU depends, of course, on the microscopic details of the grains structure and applied pressure P. We consider in the following a very simple mechanism, represented in figure 2, in which each HMU is characterized by a pair of values P_o and P_c (opening and closing pressures, respectively). These values may be different for each HMU, but always $P_o \leqslant P_c$. Plotting all the (P_c, P_o) pairs in a P_c, P_o plane generates the so-called PM representation (see two examples in figure 3).

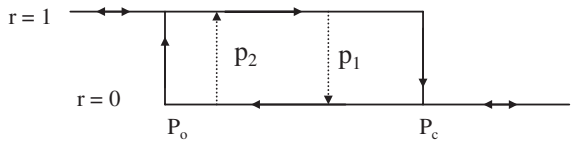

Figure 2. Dependence of the state variable r on the applied pressure P. The dashed arrows represent the transition rates between the two states $r = 1$ and 0.

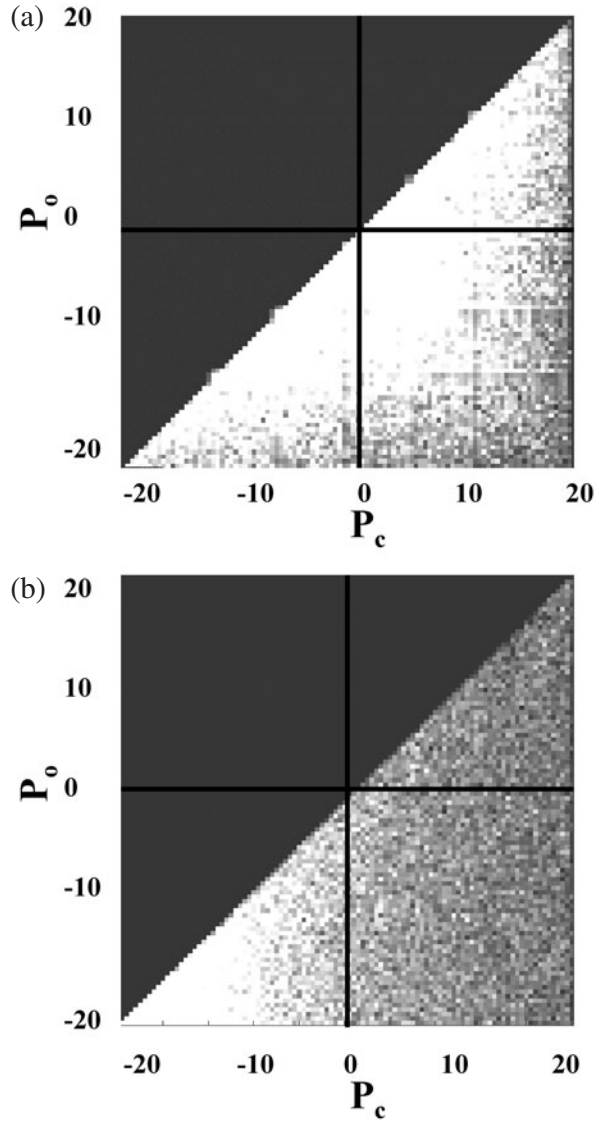

Figure 3. Two examples of PM-space density distributions (A and B). They are discussed in details in the text in section 4. Lighter gray tones denote larger densities.

Starting for any given HMU at a given pressure value $P < P_c$, we assume that $r = 1$ up to when, for $P = P_c$, it drops down to zero. Conversely, when P decreases, r remains equal to zero up to when, for $P = P_o$, it suddenly jumps to 1. In spite of its simplicity, this phenomenological model allows to reproduce all the observed effects in both quasi-static and dynamic experiments [12, 13].

In order to predict slow dynamics effects, an additional feature must be included, i.e. the possibility for $P_o < P < P_c$ of transitions from one of the two allowable states to the other. In fact, due to thermal activation, random transitions are possible with probabilities p_1 and p_2 for switching r from 1 to 0 or vice versa. These hopping transition rates increase, of course, with the temperature, but in the present context, in which only isothermal processes are considered, this dependence is not explicitly included. Likewise, any other dependence of p_1 and p_2 on, e.g. the applied pressure P is neglected. Since one can expect that the 'rigid' state be more stable than the elastic one, it is assumed that $p_1 > p_2$.

3. Quasi-static experiments

We consider in the present contribution only quasi-static experiments, in which the external stress σ, acting on the bar, is varied with time according to a certain protocol, but always leaving sufficient time between successive steps for the stress to distribute itself homogeneously through the specimen, so that the system can be assumed to be in equilibrium at any time (i.e. all time derivatives can be set to zero) and the results are independent on damping. Quasi-static conditions can be easily achieved, since the time for an ultrasonic pulse to cross the entire bar (whose length is assumed to be $\leqslant 1$ m) is of the order of 10^{-4} s, while several seconds (or even minutes) elapse between successive stress steps.

In the following, we consider virtual experiments performed with a protocol, in which the applied stress σ varies from 0 to a given $\sigma_{\max}$ in N steps $\Delta\sigma$, each of which requires T time steps, each of duration τ. The stress is then released, again in N steps $\Delta\sigma$. Since the system is in equilibrium at any time, we can write for each node during the first half cycle of the protocol

$$\begin{gathered} F_i(p\tau) = n\Delta\sigma \qquad \text{for } nT < p \leqslant (n+1)T \\ (n = 0 \cdots N,\ p = 0 \cdots NT + T) \\ P_i(p\tau) = 2F_i(p\tau) \end{gathered} \tag{10}$$

and similar equations thereafter. During each of the T time steps between two successive stress steps, the system is allowed to 'relax' under the action of the thermally activated random transitions (p_1 and p_2).

The HMU lengths $\delta_i(\sigma_t)$ may be easily calculated from equation (7). In fact, when $r_i(t) = 0$, they are unchanged from the previous values $\delta_i(\sigma_{t-1})$. When $r_i(t) = 1$, the equilibrium condition requires that $\delta_i(\sigma_t) = Q_i P_i(t)/K_i$, since $\dot{\delta}_i = 0$ and, without affecting the strain, we can assume for simplicity that $\delta_i(0) = 0$. The resulting strain of the bar can be evaluated at any time t as the sum of all the $\delta_i(\sigma_t)$ and of the grain deformations (divided by the bar rest-length L).

4. Results and discussions

In this section, we simulate the quasi-static response of a bar assumed to include 15 000 HMUs. Since in the present contribution we limit ourselves to present a few examples to illustrate qualitatively the behaviour of the system, we choose the parameters arbitrarily. Unless stated otherwise $p_1 = 0.002$, $p_2 = 0.001$ (transition probabilities per time step), $Q = 0.9$, $S = 1$, $K = 0.1$ (in arbitrary units). T has been kept as a free parameter to investigate the effect of changing

the transition rates. In fact, varying T or, by the same factor, both p_1 and p_2 yields very similar results.

As already mentioned, the distribution in the PM-space dictates the shape and width of the hysteresis loop. To show that the phenomenology described in this paper is qualitatively independent from the choice of PM-space, we consider two different representations, both suggested by a PM-space density $\rho(P_c, P_o)$ numerically determined for a Berea sandstone. In both cases (see figure 3) we have extended the density given in [16] to the $P_o < 0$ region in the PM-space:

(a) the PM density is assumed to be exponentially decaying with increasing distance from the diagonal $P_o = P_c$ and with Gaussian distribution along the diagonal:

$$\rho(P_c, P_c) = \exp(-a_1 P_c^2), \tag{11}$$

$$\rho(P_c, P_o) = \rho(P_c, P_c)\exp(-a_2(P_c - 1 - P_o)) \tag{12}$$

with $a_1 = 0.0001$ and $a_2 = 0.005$. The density is assumed to be symmetric along the line $P_c = -P_o$. This distribution in the positive pressure region is similar to the ones reported in [13, 16].

(b) Here the density is assumed to be mostly localized along the diagonal and in the lower-left corner of the PM-space, except that now the origin has been shifted down to negative pressure values. To this purpose, the distribution is chosen in such a way that $\int_{-\infty}^{P_c} \rho(P_c, P_o)\,\mathrm{d}P_o$ does not depend on the upper limit P_c and also that, for any P_c value, $\rho(P_c, P_o)$ is constant, i.e. does not depend on P_o.

Figure 4 shows the effect on the strain of many stress (or pressure) cycles, as described in the previous section, with $T = 50$. Starting from zero stress and strain and adopting the $r(t)$ scheme of figure 2, we find, for both choices of PM density (figures 4(a) and (b)), a different path in the strain–stress plane when pressure is applied or released, as expected.

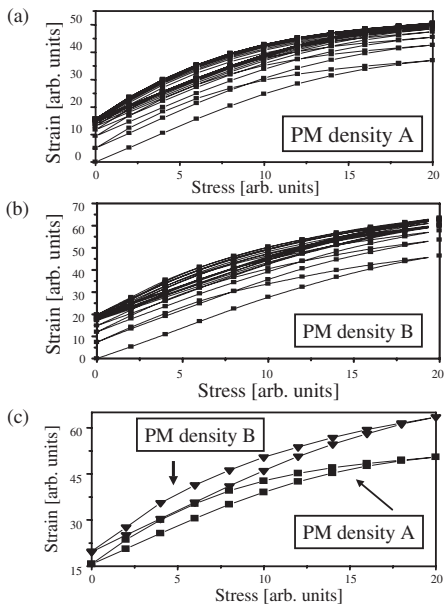

Figure 4. (a) Successive stress cycles and conditioning in the case of PM density A. (b) Successive stress cycles and conditioning in the case of PM density B. (c) Hysteretic loop at saturation for the two cases.

In addition, to this hysteretic behaviour, we observe, at the end of each stress loop, a residual strain (conditioning) due to the HMU's with $P_0 < 0 < P_c$. In fact, for those units the value of r at $P = 0$ (and therefore the value of the corresponding δ) is different in the two legs of the cycle. If $p_1 = p_2 = 0$, the second cycle would be repeated all over again in subsequent cycles, since all the parameters would remain the same. Due to the nonzero values of p_1 and p_2, however, the situation changes at each new cycle, up to when a saturation value of the residual strain is reached, i.e. the system is in equilibrium between hopping up and down events.

From that time on, the stress cycles generate stable and closed hysteretic loops (see figure 4(c)). The stable loops obtained for the two choices of the PM-space share the same characteristics (hardening and curvature). It is in fact interesting to remark that in the stable loop the curvature is always downwards, i.e. the stiffness increases with the applied stress, although less so in the upgoing branch. The larger residual strain for the case with PM density B is due to the larger number of HMU's located in the $P_o < 0$ region.

The behaviour of the residual strain as a function of time (normalized to T) is reported in figure 5(a) for the two PM densities. Again, the two curves show the same behaviour with a comparable delay in reaching the stable loop, as expected, since the delay should depend only on the experiment speed (T) and relaxation probabilities.

In figure 5(b) the residual strain is plotted vs time normalized to T for two different stress protocols for PM density B: $T = 50$ and 200. The number n of cycles needed to reach saturation is almost the same in both cases ($n = t/T \sim 6$), in agreement with the fact that, for large enough T, n should depend almost only on the transition probabilities. As a consequence, the time required to reach saturation is approximately four times larger for $T = 200$, consistent with the four times longer stress cycles. In addition, the level of residual strain reached asymptotically is much higher for $T = 50$. A simple explanation of this effect may be that, if the experiment is performed faster, there is less time

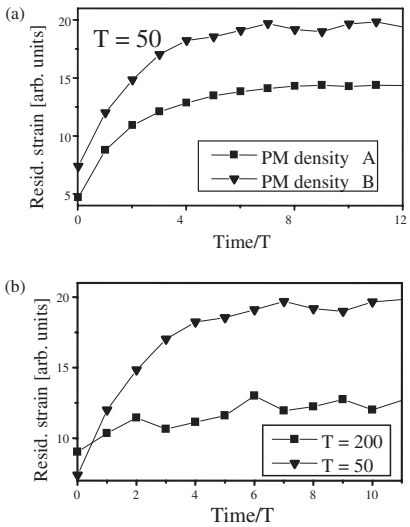

Figure 5. (a) Dependence of the residual strain on the elapsed time for the two PM densities. (b) Dependence of the residual strain on the elapsed time for two different values of T (PM density B).

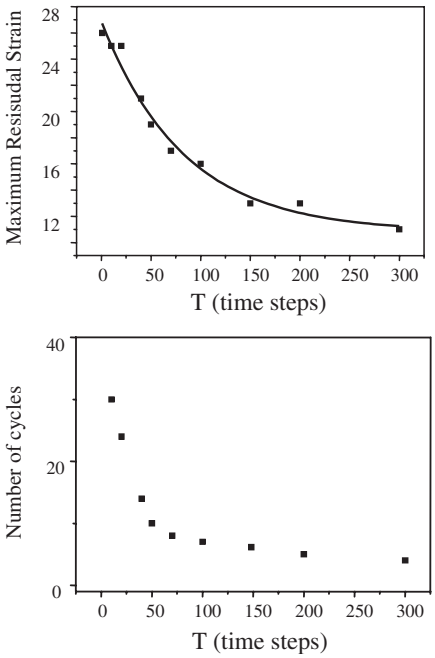

Figure 6. Maximum residual strain at saturation and approximate number of cycles needed to reach it, as functions of the time T allotted to each stress step (PM density B).

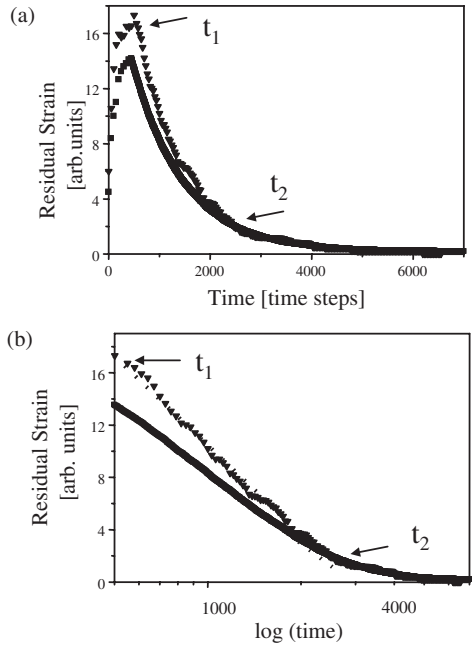

Figure 7. Time evolution of the residual strain (a) when several stress cycles are applied to the specimen, which is then left to relax; (b) during relaxation vs $\log(t)$. PM density A: ●; PM density B: ▼.

available for relaxation between successive experiments and, as a consequence, more residual strain is accumulated. In both cases, the numerical data can be fitted well with an exponential increase of the residual strain with time towards a saturation value.

In figure 6, the maximum residual strain (i.e. the strain at zero stress for the saturation cycle) and the approximate number of cycles needed to reach it, are plotted vs T. Again, we find an exponential curve fitting for the maximum residual strain, which decreases when the experiment is performed more slowly. Also, for slow enough experiments (large T), the number of cycles is almost constant, as already remarked.

In figure 7, we consider the temporal evolution of the residual strain when several stress cycles are applied to the specimen, which is then left to relax. Initially the residual strain increases with time, as it could already be seen in figure 4(a) (for $\sigma = 0$), until saturation is reached. Then no further stress cycles are applied and thermal relaxation brings the system back to the original zero strain condition. In agreement with experimental results, the process is very slow. In figure 7(b) the decay part of the curve is plotted vs the logarithm of time. The result seems to be a straight line between the times t_1 and t_2. The behaviour is similar for both PM distributions.

To our knowledge, the relaxation process in quasi-static experiments has not yet been studied. However, preliminary data on Berea sandstone seem to indicate the existence of a residual deformation when the stress is removed (i.e. at the end of the loading–unloading cycle), which recovers logarithmically with time [17]. Also, experimental evidence has been found for a $\log(t)$ recovery in resonant dynamic experiments [2, 6].

In figure 8, we study the effect of relaxation at a fixed stress. To this purpose, we simulate a succession of stress

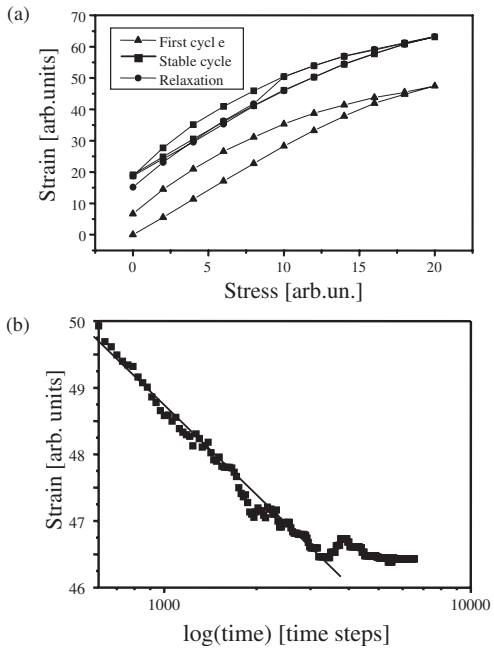

Figure 8. (a) The first and the stable cycles are shown, and also the behaviour after relaxation at $\sigma = 10$ a.u. (b) Strain vs $\log(t)$ during relaxation at $\sigma = 10$ a.u. (PM density B).

cycles until saturation is reached. Then, we perform an additional cycle in which, when $\sigma = 10$ a.u. and in the downgoing branch, the system is left to relax for a very long time keeping the stress fixed. The temporal evolution of the strain during relaxation, shown in figure 8(b), exhibits again a $\log(t)$ decay. After relaxation, the stress cycle is completed down to zero stress (see figure 8(a)). As a consequence, the strain falls down to a loop corresponding to a previous stress cycle, in agreement with experimental observations.

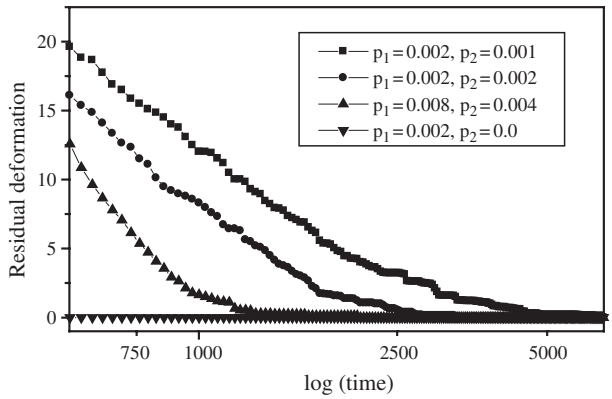

Figure 9. Residual strain during relaxation after conditioning vs $\log(t)$ for different values of the transition probabilities (PM density B).

Finally, in figure 9, we analyse the effects of different choices for the ratio p_1/p_2 on the relaxation of the residual strain (PM density B). As expected, no residual strain and no relaxation are observed when $p_2 = 0$. In fact, HMUs with $P_o < 0$ are all initially rigid and remain rigid during the entire compression experiment. In all other cases, a complete recovery is observed, with a logarithmic behaviour during a long time interval. Recovery is faster when the probability p_1 is larger.

5. Conclusions

A model has been recently proposed for the simulation of nonclassical nonlinear effects in quasi-static [13] and resonant dynamics [12] experiments. The model is based on a description of the specimen (a bar made of a multi-grained material) as a sequence of elastic grains and interstices (called hysteretic mesoscopic units). The latter are assumed to be responsible for the nonclassical nonlinear properties of the specimen and own their hysteretic behaviour to a two-valued state variable $r(t)$.

In this contribution, the model is further enriched by the inclusion of thermally activated random transitions between the two values of the state variable. As a consequence, various experimental observations, such as the conditioning of the specimen under the effect of a sequence of quasi-static stress cycles and its very slow return to the initial conditions when the stress is released, are well reproduced. In addition, several predictions are made, which could be easily verified experimentally. Among them:

(a) Figure 6(b) predicts the number of cycles required to reach saturation for different values of the time elapsed in each stress step.
(b) Figure 7(b) suggests a logarithmic relaxation of the residual strain, analogous to the logarithmic recovery in slow dynamics experiments.
(c) Figure 8(b) predicts a similar logarithmic relaxation also at fixed stress.

Of course all these predictions are merely qualitative, since the values of the parameters p_1 and p_2 are not known. In fact, quasi-static experiments to verify the predictions of the model would be extremely useful to confirm the validity of the proposed mechanism of thermally activated random transitions (or else to suggest modifications thereof) and to evaluate the corresponding parameters. It is important to note that the above mentioned predictions are qualitatively independent of the details of the underlying basic model and stress protocol, but rely substantially on the mechanism of hopping transitions between the two values of $r(t)$.

Acknowledgments

This work was supported by MURST and by the INFM Parallel Computing Initiative (Italy). We are also indebted to the European Science Foundation for support through the programme NATEMIS. One of us (PPD) wishes to thank Prof. C Condat for useful discussions.

References

[1] Guyer R A and Johnson P A 1999 *Phys. Today* **52** 30
[2] Guyer R A, Tencate J A and Johnson P A 1999 *Phys. Rev. Lett.* **82** 3280–3
[3] TenCate J A, VanDenAbeele K E-A, Shankland T J and Johnson P A 1996 *J. Acoust. Soc. Am.* **99** 3334–45
[4] Guyer R A, McCall K R and Boitnott G N 1995 *Phys. Rev. Lett.* **74** 3491
[5] TenCate J A and Shankland T J 1996 *Geophys. Res. Lett.* **23** 3019–22
[6] TenCate J A, Smith E and Guyer R A 2000 *Phys. Rev. Lett.* **85** 1020–4
[7] Heslot F, Baumberger T, Perrin B, Caroli B and Caroli C 1994 *Phys. Rev.* E **49** 4973
Fischer K H and Hertz J A 1991 *Spin Glasses* (Cambridge: Cambridge University Press) p 8
[8] Van den Abeele K, Johnson P A and Sutin A 2000 *Research on Nondestructive Evaluation* **12** 17–30
[9] Landau L D and Lifshitz E M 1986 *Theory of Elasticity* (Oxford: Pergamon)
[10] VanDenAbeele K E-A, Johnson P A, Guyer R A and McCall K R 1997 *J. Acoust. Soc. Am.* **101** 1885–98
[11] McCall K R and Guyer R A 1996 *Non Linear Process. Geophys.* **3** 89–101
[12] Agostini V, Delsanto P P, Johnson P A, Van den Abeele K and Scalerandi M 2002 *J. Acoust. Soc. Am.* submitted
Delsanto P P, Agostini V, Scalerandi M and Johnson P A 2000 Phenomenology and modeling of damaged mesoscopic materials *Proc. Euromech 419 Conf. (Praga)* at press
[13] Ruffino E and Scalerandi M 2000 *Il Nuovo Cimento* B **115** 645–52
[14] Delsanto P P, Mignogna R, Scalerandi M and Schechter R 1998 Simulation of ultrasonic pulse propagation in complex media *New Perspectives on Problems in Classical and Quantum Physics* vol 2, ed P P Delsanto and A W Saenz (New Delhi: Gordon & Breach) pp 51–74
[15] Delsanto P P and Scalerandi M 1998 *J. Acoust. Soc. Am.* **104** 2584–91
[16] Guyer R A, McCall K R, Boitnott G N, Hilbert L B and Plona T J 1997 *J. Geoph. Res.* **102** 5281
[17] Van Den Abeele K Private communication